3-14-2018

3D multilevel spin transfer torque devices

J. Hong
Huazhong University of Science and Technology

M. Stone
Department of Electrical and Computer Engineering, Florida International University

Department of Electrical and Computer Engineering, Florida International University

K. Luongo
Department of Electrical and Computer Engineering, Florida International University

Q. Zheng
Beijing Normal University

See next page for additional authors

Authors
J. Hong; M. Stone; Department of Electrical and Computer Engineering, Florida International University; K. Luongo; Q. Zheng; Z. Yuan; K. Xia; N. Xu; L. You; and Sakhrat Khizroev

APPLIED PHYSICS LETTERS **112**, 112402 (2018)

3D multilevel spin transfer torque devices

J. Hong,[1,a),b)] M. Stone,[2,a)] B. Navarrete,[2] K. Luongo,[2] Q. Zheng,[3] Z. Yuan,[3] K. Xia,[3] N. Xu,[4] J. Bokor,[4] L. You,[1,b)] and S. Khizroev[2]

[1]*School of Optical and Electronic Information, Huazhong University of Science and Technology, Wuhan, Hubei 430074, People's Republic of China*
[2]*Department of Electrical and Computer Engineering, Florida International University, Miami, Florida 33174, USA*
[3]*Department of Physics, Beijing Normal University, Beijing 100875, People's Republic of China*
[4]*EECS, University of California-Berkeley, Berkeley, California 94720, USA*

(Received 3 January 2018; accepted 3 March 2018; published online 14 March 2018)

Spin-transfer torque magnetic tunneling junction devices capable of a multilevel three-dimensional (3D) information processing are studied in the sub-20-nm size range. The devices are built using He^+ and Ne^+ focused ion beam etching. It has been demonstrated that due to their extreme scalability and energy efficiency, these devices can significantly reduce the device footprint compared to the modern CMOS approaches and add advanced features in a 3D stack with a sub-20-nm size using a spin polarized current. *Published by AIP Publishing.* https://doi.org/10.1063/1.5021336

The need for energy-efficient computing nowadays is more urgent than ever before, covering various domains such as large-scale sensor networks,[1] Internet of Things (IoT),[2] bioelectronics,[3] and neuromorphic/neuro-inspired computing.[4] With the dramatic increase in device counts to meet the modern system requirements,[1,4,5] it is critical to develop a building block with fundamentally different computing and storage mechanisms.[6] Non-volatile switches with novel computing mechanisms are considered as the most promising solution to overcome the energy brick wall.[7–11] Among them, spin-based technologies have advantages of non-volatile memory and logic owing to their supreme features of low-voltage (sub-1 V), high-speed operation (sub-ns), and high endurance (over 10^{12} cycles).[12–14] Spintronic devices consist of reading and writing nanomagnets. The information is read back through the tunneling magnetoresistance (TMR) while it is written by any of these methods, including application of a magnetic field, a spin-transfer torque (STT), a spin-orbit torque (SOT), a current induced magnetic domain wall motion (DWM), or an electric field-controlled magnetic anisotropy (VCMA) effect.[15–18] Amongst existing demonstrations, a tri-layer magnetic tunneling junction (MTJ) using the STT effect to switch its magnetic configuration between parallel (P) and anti-parallel (AP) states could achieve multi-level signal processing with relatively high energy efficiency. Some of the most advanced studies in the field have reported STT-MTJ devices with a characteristic size in the sub-20-nm range.[19–22] First commercial products based on the STT technology and known as STT-MRAM in low-power platforms have appeared as a replacement to S/DRAM-based cache.[23] Recently, integration of the spintronic non-volatility with process-in-memory (PIM) has also been suggested as a promising solution to resolve the "von Neumann bottleneck" issues.[24–27]

Another significant opportunity for the STT technology would be to exploit the "multi-level per bit" capability, also known as "multiple level per cell" (SLC or MLC).[28] From this motivation, we investigate a dual-MTJ-in-series structure using variable sized sub-20-nm single-domain magnets with perpendicular magnetic anisotropy (PMA).

In this study, we fabricated all-free layered magnetic junctions in which each layer switches either "up" or "down" in the perpendicular direction. The all-free layer configuration is not only relatively easy to fabricate but has an advantage of a straightforward operation. To induce perpendicular magnetic anisotropy (PMA), well-established Ta/CoFeB/MgO stacks were used.[19,29] For increasing the interface anisotropy of the second magnetic layer, dual stacks of MgO were deposited.[30–32] For the programming of the device structures, the purely clean structures were fabricated with identical island stacks. To program such memory devices, the STT switching was implemented to switch magnets one by one, as described below in more detail. The coercivity values of the three magnets were varied through the deposition conditions for the three layers, respectively.

Figure 1(a) shows a schematic of the three-layer magnetic tunneling junction. The net resistance of this device is defined by two junctions in series, with the resistance of each junction defined by the TMR effect, i.e., by the relative orientation of the magnetization in the two adjacent layers. In this configuration, each of the three magnetic layers effectively acts as a free layer with a magnetization directed up or down. The relative switching is produced through the STT effect. As a result, the two junctions placed in series should produce at least ternary information processing, as described below in more detail.

Particularly, due to the recent progress of e-beam lithography (EBL) of magnetic thin film stacks, magnetic devices could be patterned down to sub-10-nm range for mass production of next generation spintronic devices.[33] However, for the sake of demonstration, focused ion beam (FIB) is an appropriate fabrication tool. Although challenging for mass production, FIB is an ideal tool for fabrication of sub-10-nm individual prototype devices. Thanks to the recent development of multi-beam FIB using He^+ and Ne^+ ions, besides the traditional Ga+ ions, FIB has become a viable prototyping approach.[34,35]

[a)]J. Hong and M. Stone contributed equally to this work.
[b)]Authors to whom correspondence should be addressed: jeongmin.hong@gmail.com or lyou@hust.edu.cn

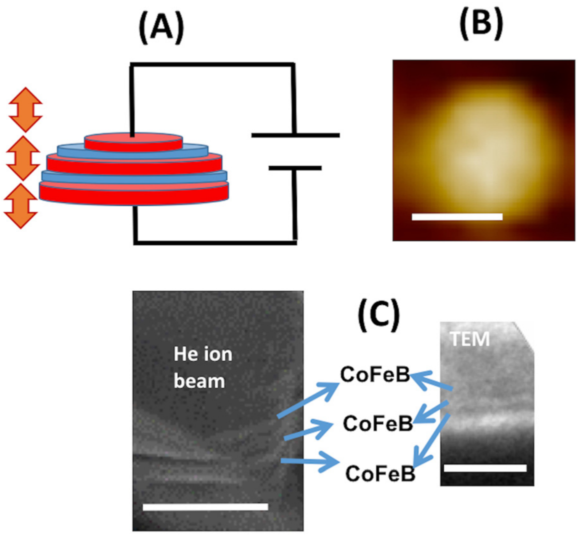

FIG. 1. Schematics of the geometry of (a) 3D multilevel MTJs. (b) Atomic force microscopy (AFM) image of the 3D MTJs. The scale bar is 10 nm. (c) Helium ion beam micrograph (HIM) and transmission electron micrograph (TEM) image of the sub-20-nm island stack. The scale bars are 10 nm.

The layer composition of the dual MTJ structure starting from the substrate is Ta/Ru/Ta/CoFeB(M_1)/MgO/CoFeB(M_2)/MgO/CoFeB(M_3)/Ta. Figure 1(b) presents a high-resolution transmission electron microscopy (TEM) image of a cross-section of the dual-junction MTJ device with a sub-20-nm planar elliptical side fabricated with the He+ beam. The TEM image shows the three magnets and the two insulating layers to be in the sub-1-nm size range. In Fig. 1(c), an atomic force microscopy (AFM) image shows the device to have an elliptical shape with a characteristic diameter of 17 ± 2 nm. The scale bar is 10 nm. The errors of the size variation from imaging measurement tools have been found in the literature.[7]

Ultra-high sensitive MOKE measurements were performed to characterize the dual junction stack, as shown in Fig. 2(a).[7] According to the m-H loop measurements, the magnetization in the three magnetic layers switches sequentially through the application of a magnetic field. The variation in the coercivity, H_C, between three layers was achieved by a variation in the thickness by approximately 50% between the layers. The values were defined by the thickness of each layer, 1, 1.3, and 1.6 nm, respectively. The measured coercivity of the three layers was approximately 20, 40, and 50 Oe from the top magnet, respectively. The characteristic planar size of the multilevel bit was on the order of 17 ± 2 nm as shown in Fig. 2(b). The saturation magnetization, $\boldsymbol{M_S}$, for the magnetic layers was on the order of 500 emu/cc, the anisotropy energy, $\boldsymbol{K_U}$, was on the order of 1.1. MJ/m^3, and the thickness of the insulating MgO layer was on the order of 1 nm.

We performed field-applied magnetic force microscopy (FA-MFM) measurements to probe the sub-20-nm structures, as shown in Fig. 2(b). Four distinct MFM signal levels can be detected through FA-MFM. The magnetic fields are carefully applied in the perpendicular direction to trace magnetization switching in each magnet. It could be noted that the three layers of the dual-MTJs could switch one by one.

The model structure for I-V measurements is shown in Fig. 3(a). It can be represented as two junction resistances, R^1 and R^2, respectively, in series. Here, R^1 is the resistance of the interface between magnets M_1 and M_2, while R^2 is the resistance of the interface between magnets M_2 and M_3. Figure 3(b) shows an illustration of 8 possible spin configurations that correspond to three distinct relative spin orientations at the two junctions: (1) the lowest resistance value when both junctions have parallel orientations (P/P), (2) the middle resistance value when the two junctions have parallel and antiparallel relative orientations (P/AP or AP/P combinations), and (3) the highest resistance value when both junctions have antiparallel orientations (AP/AP).

Indeed, as shown in Fig. 3(c), the I-V curve clearly shows three resistance values, 46, 52, and 82 kΩ, respectively. This I-V curve was obtained by using voltage as the driving source.[18,36] Figure 3(d) shows a control sequence of voltage applications to move the spin configuration from one state to another within a closed loop by sweeping voltage, starting from zero to +100 mV, then reversing from +100 to −100 mV, and then increasing from −100 mV back to zero. The "up" and "down" spin orientations are coded as red and blue, respectively. The experiment shows a straightforward sequence of voltages/currents to switch between the three resistance values. The sequence is very straightforward and based on the symmetry consideration.

Using an example of a two-junction MTJ device, this study clearly demonstrated that the STT effect could be used to switch relative spin orientations in a MTJ device with more than one junction. The STT switching current density on the order of 3 MA/cm^2 was comparable to the values in typical sub-20-nm single-junction MTJs as reported elsewhere.[19,37–39] It can be noted that for this particular geometry and parameters' setup, the states in which both junctions have antiparallel spins (AP/AP) exist only in a relatively narrow voltage range (∼3 mV) or, in other words, these states

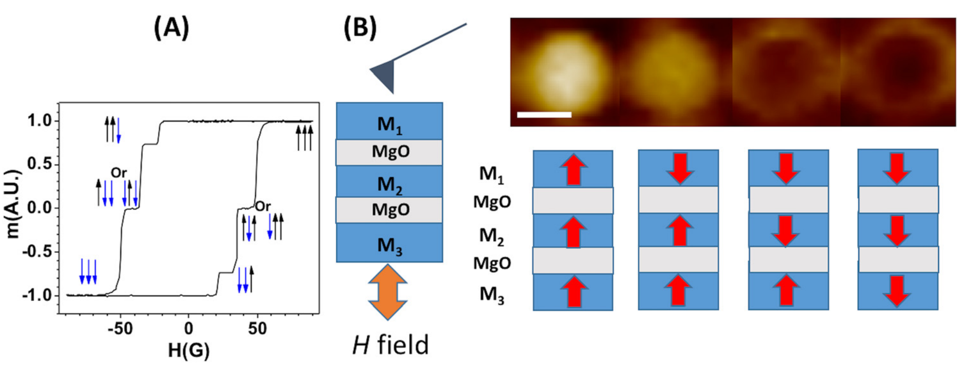

FIG. 2. Magnetic properties of MTJ structures. (a) m-H loops of the structures. (b) Field-applied MFM (magnetic force microscopy) measurement of the sub-20-nm (∼17 ± 2 nm) of dual magnetic tunneling junction structures.

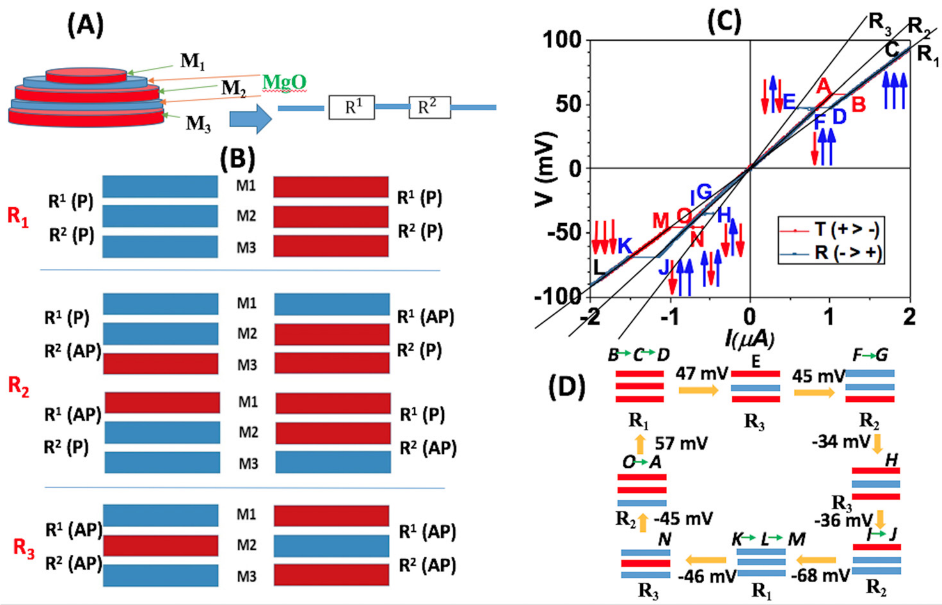

FIG. 3. I-V characteristics of the device. (a) Two resistance model and possible configurations. (b) Possible scenario of the switching mechanism. (c) I-V measurement data of the device. (d) Switching process of the dual MTJs from the experiment.

are not relatively stable for this particular set of coercivity fields. However, it should be understood that if necessary, this state can be made as stable as the other layers by increasing its coercivity, as explained below in more detail. These states are denoted as *E*, *H*, and *N* in Figs. 3(c) and 3(d). This could be explained by the fact that for these states, the middle layer must have the spin orientation opposite to the spin orientations in the two side layers. Therefore, in these cases, the demagnetization field in the middle layer reaches its highest possible value compared to all the other spin states (with only one or no AP junction). Given the saturation magnetization of 500 emu/cc, the demagnetization field in these AP/AP states would be on the order of 500 Oe. Therefore, to make these AP/AP states more stable, the magnetocrystalline anisotropy energy could be further increased either by deposition conditions or using different materials. Also, it is noteworthy that the "voltage" was always applied in the direction to switch one layer at a time, as shown in the control sequence loop diagram in Fig. 3(d). It would be possible to extend this approach to switch even more than three magnetic layers by the STT effect through a multi-junction MTJ structure with more than two junctions.

In summary, 3D multilevel operation of a MTJ with low switching energy has been clearly proposed and performed using dual MTJ stacks switched through the STT effect. This type of nanomagnetic junction with multilevel signal processing could be immediately used for future 3D electronics, memristors, and PIM applications. Also, it could be programmable and compatible with the current CMOS technology. The results could pave the way for future spin devices.

CoFeB magnets and MgO insulation layers are deposited through a Pateo series 7-guns sputtering system manufactured from K-Lab Co., Ltd. (S. Korea). The base pressure was as low as 2.0×10^{-8} Torr, and the process pressure range was varied between 0.5 mTorr and 5 mTorr. The annealing temperature has been increased up to 800 K. A high-quality and high-density MgO target was provided by Ube Industries Co., Ltd. (Japan). The process pressure, gas flow, power, and time have been optimized for the deposition of the ideal structures.

Scanning probe microscopy (SPM) was performed in the non-contact mode using a Bruker-Nano AFM system. The MFM measurements were conducted in a dynamic lift mode with a lift distance of 20 and 30 nm. The ultra-high sensitivity magnetic tip was fabricated. The dynamics were measured under the presence of a magnetic field by sweeping the magnetic field range in the perpendicular direction.

The high sensitive MOKE measurement was performed using a home-made focused MOKE system. A 635-nm diode laser was directed toward the sample, which was located between the poles of a vector magnet. The magnetic field at the probe spot was calibrated using a three-axis Hall probe sensor (C-H3A-2m Three Axis Magnetic Field Transducer, SENIS GmbH Zürich, Switzerland). The accuracy of the magnetic field measurement is estimated to be ~1%. The time to sweep full hysteresis loops was 20 min (5 Oe/s).

The programmable transport measurement was performed using a home-made measurement setup which could perform high sensitivity transport measurements such as delta-mode experiment. The sample was mounted on a chip carrier after being carefully wire bonded and inside a Faraday cage to reduce the possible noises during the measurement.

This work was supported by the National Natural Science Foundation of China under Award No. 61674062. The authors acknowledge financial support from the Office of Naval Research (ONR) No. 11594311 and the National Science Foundation (NSF) Nos. 0939514 and NSF-IIP 1237818. The work at the Molecular Foundry (TMF) was supported by the U.S. Department of Energy, Office of Basic Energy Sciences, Division of Materials Sciences and Engineering under Contract No. DE-AC02-05CH11231. The authors acknowledge the consulting support for process optimization of the conditions for the deposition of magnets and oxide layers from K-Lab Co., Ltd.

[1]A. W. Holger, *Protocols and Architectures for Wireless Sensor Networks* (John Wiley & Sons, 2007), ISBN: 978-0-470-51923-3.
[2]J. Gubbi, R. Buyya, S. Marusic, and M. Palaniswami, "Internet of Things (IoT): A vision, architectural elements, and future directions," Future Gener. Comput. Syst. **29**, 1645–1660 (2013).

[3]A. Szent-Gyorgyi, "Bioelectronics," Science **161**, 988–990 (1968).
[4]J. J. Hopfield, "Neural networks and physical systems with emergent collective computation abilities," Proc. Natl. Acad. Sci. U. S. A. **79**, 2554–2558 (1982).
[5]J. D. Owens, M. Houston, D. Luebke, S. Green, J. E. Stone, and J. C. Philips, "GPU computing," Proc. IEEE **96**, 879–899 (2008).
[6]J. V. Barth, G. Constantini, and K. Kern, "Engineering atomic and molecular nanostructure at surfaces," Nature **437**, 671–679 (2005).
[7]J. Hong, B. Lambson, S. Dhuey, and J. Bokor, "Experimental test of Landauer's principle in single-bit operations on nanomagnetic memory bits," Sci. Adv. **2**, e1501492 (2016).
[8]S. A. Wolf, D. D. Awschalom, R. A. Buhman, J. M. Daughton, S. von Molnar, M. L. Roukes, A. Y. Chtchelkanova, and D. M. Treger, "Spintronics: A spin-based electronics vision for the future," Science **294**, 1488–1495 (2001).
[9]A. Peschot, C. Qian, and T.-J. King Liu, "Nanomechanical switches for low-power digital computing," Micromachines **6**, 1046–1065 (2015).
[10]C. H. van der Wal, A. C. J. ter Haar, F. K. Wilhelm, R. N. Schouten, C. J. P. M. Harmans, T. P. Orlando, S. Lloyd, and J. E. Mooij, "Quantum superposition of macroscopic persistent-current states," Science **290**, 773–777 (2000).
[11]T. Hasegawa, K. Terabe, T. Tsuruoka, and M. Aono, "Atomic switch: Atom/ion movement controlled devices for beyond von-neumann computers," Adv. Mater. **24**, 252–267 (2012).
[12]J. O. Lee, Y.-H. Song, M.-W. Kim, M.-H. Kang, J.-S. Oh, H.-H. Yang, and J.-B. Yoon, "A sub-1-volt nanoelectromechanical switching device," Nat. Nanotechnol. **8**, 36–40 (2013).
[13]D. Loke, T. H. Lee, W. J. Wang, L. P. Shi, R. Zhao, Y. C. Yeo, T. C. Chong, and S. R. Elliott, "Breaking the speed limits of phase-change memory," Science **336**, 1566–1569 (2012).
[14]M.-J. Lee, C. B. Lee, D. Lee, S. R. Lee, M. Chang, J. H. Hur, Y.-B. Kim, C.-J. Kim, D. H. Seo, S. Seo, U.-I. Chung, I.-K. Yoo, and K. Kim, "A fast, high-endurance and scalable non-volatile memory device made from asymmetric Ta2O5-X/TaO2-X bilayer structures," Nat. Mater. **10**, 625–630 (2011).
[15]D. C. Ralph and M. D. Stiles, "Spin transfer torques," J. Magn. Magn. Mater. **320**, 1190–1216 (2008).
[16]D. Bhowmik, L. You, and S. Salahuddin, "Spin Hall effect clocking of nanomagnetic logic without a magnetic field," Nat. Nanotechnol. **9**, 59–63 (2014).
[17]I. M. Miron, T. Moore, H. Szambolics, L. D. Buda-Prejbeanu, S. Auffret, B. Rodmacq, S. Pizzini, J. Vogel, M. Bonfim, A. Schuhl, and G. Gaudin, "Fast current-induced domain-wall motion controlled by the Rashba effect," Nat. Mater. **10**, 419–423 (2011).
[18]S. Kanai, M. Yamanouchi, S. Ikeda, Y. Nakatani, F. Matsukura, and H. Ohno, "Electric field induced magnetization reversal in a perpendicular-anisotropy CoFeB-MgO magnetic tunnel junction," Appl. Phys. Lett. **101**, 122403 (2012).
[19]H. Sato, S. Ikeda, and H. Ohno, "Magnetic tunnel junctions with perpendicular easy axis at junction diameter of less than 20 nm," Jpn. J. Appl. Phys., Part 1 **56**, 0802A6 (2017).
[20]S. Ikeda, K. Miura, H. Yamamoto, K. Mizunuma, H. D. Gan, M. Endo, S. Kanai, J. Hayakawa, F. Matsukura, and H. Ohno, "A perpendicular-anisotropy CoFeB-MgO magnetic tunnel junction," Nat. Mater. **9**, 721–724 (2010).
[21]M. Gajek, J. J. Nowak, J. Z. Sun, P. L. Trouilloud, E. J. O'Sullivan, D. W. Abraham, M. C. Gaidis, G. Hu, S. Brown, Y. Zhu *et al.*, "Spin troque switching of 20 nm magnetic tunnel junctions with perpendicular anisotropy," Appl. Phys. Lett. **100**, 132408 (2012).
[22]S. Chen, C. Qin, and Y. Ji, "Asymmetric spin absorption into a nonlocal spin detector," J. Appl. Phys. **118**, 033901 (2015).
[23]See http://www.eenewsanalog.com/news/fdsoi-getembedded-mram-flash-options-28nm-0 for "Samsung's eMRAM in 28 FDSOI."
[24]S. Fujita, H. Noguchi, K. Ikegami, S. Takeda, K. Nomura, and K. Abe, "Novel STT-MRAM based last level caches for high performance processors using normally-off architectures," in *2014 International Symposium on Integrated Circuits*, Singapore (2014), pp. 316–319.
[25]J. J. Pieper, A. Mellan, J. M. Paul, D. E. Thomas, and F. Karim, "High level cache simulation for heterogeneous multiprocessors," in *Proceedings of the 41st Design Automation Conference*, San Diego, CA, USA (2004), pp. 287–292.
[26]B. R. Zeydel, D. Baran, and V. G. Oklobdzija, "Energy-efficient design methodologies: High-performance VLSI adders," IEEE J. Solid-State Circuits **45**, 1220–1233 (2010).
[27]B. Gassend, G. E. Suh, D. Clarke, M. van Dijk, and S. Devadas, "Caches and hash trees for efficient memory integrity verification," in *Proceedings of the Ninth International Symposium on High-Perfomance Computer Architecture*, HPCA-9 2003 (2003), pp. 295–306.
[28]S. Lequeux, J. Sampaio, V. Cros, K. Yakushiji, A. Fukushima, R. Matsumoto, H. Kubota, S. Yuasa, and J. Grollier, "A magnetic synapse: Multilevel spin-torque memristor with perpendicular anisotropy," Sci. Rep. **6**, 31510 (2016).
[29]D. C. Worledge, G. Hu, D. W. Abraham, J. Z. Sun, P. L. Trouilloud, J. Nowak, S. Brown, M. C. Gaidis, E. J. O'Sullivan, and R. P. Robertazzi, "Spin torque switching of perpendicular Ta | CoFeB | MgO-based magnetic tunnel junctions," Appl. Phys. Lett. **98**, 022501 (2011).
[30]H. Gan, S. Ikeda, M. Yamanouchi, K. Miura, K. Mizunuma, J. Hayakawa, F. Matsukura, and H. Ohno, "Tunnel magnetoresistance properties of double MgO-barrier magnetic tunnel junctions with different free-layer alloy compositions and structures," IEEE Trans. Mag. **47**, 1567 (2011).
[31]G. Feng, S. van Dijken, J. F. Feng, J. M. D. Coey, T. Leo, and D. J. Smith, "Annealing of CoFeB/MgO based single and double barrier magnetic tunnel junctions: Tunnel magnetoresistance, bias dependence, and output voltage," J. Appl. Phys. **105**, 033916 (2009).
[32]H. Kubota, S. Ishibashi, T. Saruya, T. Nozaki, A. Fukushima, K. Yakushiji, K. Ando, Y. Suzuki, and S. Yuasa, "Enhancement of perpendicular magnetic anisotropy in FeB free layers using a thin MgO cap layer," J. Appl. Phys. **111**, 07C723 (2012).
[33]B. Lee, J. Hong, N. Amos, I. Dumer, D. Litvinov, and S. Khizroev, "Sub-10-nm-resolution electron-beam lithography toward very-high-density multilevel 3D nano-magnetic information devices," J. Nanopart. Res. **15**, 1665 (2013).
[34]F. Watt, A. A. Bettiol, J. A. van Kan, and M. B. H. Breese, "Ion beam lithography and nanofabrication: A review," Int. J. Nanosci. **4**, 269–286 (2005).
[35]S. Khizroev and D. Litvinov, "Focused-ion-beam-based rapid prototyping of nanoscale magnetic devices," Nanotechnology **14**, R7–R15 (2004).
[36]C. Yoshida, H. Noshiro, Y. Yamazaki, T. Sugii, T. Tanaka, A. Furuya, and Y. Uehara, "Micromagnetic simulation of electric-field-assisted magnetization switching in perpendicular magnetic tunnel junction," AIP Adv. **7**, 055935 (2017).
[37]J. Hong, A. Hadjikhani, M. Stone, F. I. Allen, V. Safonov, P. Liang, J. Bokor, and S. Khizroev, "The physics of spin transfer torque switching in magnetic tunneling junctions in sub-10-nm size range," IEEE Trans. Magn. **52**, 1400504 (2016).
[38]J. Hong, P. Liang, V. L. Safonov, and S. Khizroev, "Energy-efficient spin-transfer torque magnetization reversal in sub-10-nm magnetic tunneling junction point contacts," J. Nanopart. Res. **15**, 1599 (2013).
[39]H. Sato, E. C. I. Enobio, M. Yamanouchi, S. Ikeda, S. Fukami, S. Kanai, F. Matsukura, and H. Ohno, "Properties of magnetic tunnel junctions with a MgO/CoFeB/Ta/CoFeB/MgO recording structure down to junction diameter of 11 nm," Appl. Phys. Lett. **105**, 062403 (2014).